Institute of Paper Science and Technology
Atlanta, Georgia

IPST Technical Paper Series Number 853

Scale and Boundary Conditions Effects in Elastic Properties of Random Composites

M. Jiang, K. Alzebdeh, I. Jasiuk, and M. Ostoja-Starzewski

May 2000

Submitted to
Acta Mechanica

INSTITUTE OF PAPER SCIENCE AND TECHNOLOGY
PURPOSE AND MISSIONS

The Institute of Paper Science and Technology is an independent graduate school, research organization, and information center for science and technology mainly concerned with manufacture and uses of pulp, paper, paperboard, and other forest products and byproducts. Established in 1929 as the Institute of Paper Chemistry, the Institute provides research and information services to the wood, fiber, and allied industries in a unique partnership between education and business. The Institute is supported by 52 North American companies. The purpose of the Institute is fulfilled through four missions, which are:

- to provide multidisciplinary graduate education to students who advance the science and technology of the industry and who rise into leadership positions within the industry;
- to conduct and foster research that creates knowledge to satisfy the technological needs of the industry;
- to provide the information, expertise, and interactive learning that enables customers to improve job knowledge and business performance;
- to aggressively seek out technological opportunities and facilitate the transfer and implementation of those technologies in collaboration with industry partners.

ACCREDITATION

The Institute of Paper Science and Technology is accredited by the Commission on Colleges of the Southern Association of Colleges and Schools to award the Master of Science and Doctor of Philosophy degrees.

NOTICE AND DISCLAIMER

The Institute of Paper Science and Technology (IPST) has provided a high standard of professional service and has put forth its best efforts within the time and funds available for this project. The information and conclusions are advisory and are intended only for internal use by any company who may receive this report. Each company must decide for itself the best approach to solving any problems it may have and how, or whether, this reported information should be considered in its approach.

IPST does not recommend particular products, procedures, materials, or service. These are included only in the interest of completeness within a laboratory context and budgetary constraint. Actual products, materials, and services used may differ and are peculiar to the operations of each company.

In no event shall IPST or its employees and agents have any obligation or liability for damages including, but not limited to, consequential damages arising out of or in connection with any company's use of or inability to use the reported information. IPST provides no warranty or guaranty of results.

SCALE AND BOUNDARY CONDITIONS EFFECTS IN ELASTIC PROPERTIES OF RANDOM COMPOSITES

M. Jiang[1], K. Alzebdeh[2], I. Jasiuk[1] and M. Ostoja-Starzewski[3]

[1]The George W. Woodruff School of Mechanical Engineering
Georgia Institute of Technology
Atlanta, GA 30332-0405

[2]Ergotron Inc.
Minneapolis, MN 55121

[3]Institute of Paper Science and Technology, and Georgia Institute of Technology
500 10th Street, N.W.
Atlanta, GA 30318-5794

Abstract

We study elastic anti-plane responses of unidirectional fiber-matrix composites. The fibers are of circular cylinder shape, aligned in the axial direction, and arranged randomly, with no overlap, in the transverse plane. We assume that both fibers and matrix are linear elastic and isotropic. In particular, we focus on the effects of scale of observation and boundary conditions on the overall anti-plane (axial shear) elastic moduli. We conduct this analysis numerically, using a two-dimensional square spring network, at the mesoscale level. More specifically, we consider finite "windows of observation," which we increase in size. We subject these regions to several different boundary conditions: displacement-controlled, traction-controlled, periodic, and mixed (combination of any of the first three) to evaluate the mesoscale moduli. The first two boundary conditions give us scale-dependent bounds on the anti-plane elastic moduli. For each boundary condition case we consider many realizations of the random composite to obtain statistics. In this parametric study we cover a very wide range of stiffness ratios ranging from composites with very soft inclusions (approximating holes) to those with very stiff inclusions (approaching rigid fibers), all at several volume fractions.

---

to be published in *ACTA MECHANICA*

1. Introduction

A key role in continuum mechanics is played by the concept of a representative volume element (RVE). Interestingly, however, the RVE has hardly been studied prior to the nineties. Given the ever so stronger preoccupation of solid mechanics research with the microstructural effects, the situation is now changing. The starting point is offered by the definition of Hill [1], according to which the RVE refers to "*a sample that (i) is structurally entirely typical of the whole mixture on average, and (ii) contains a sufficient number of inclusions for the apparent overall moduli to be effectively independent of the surface values of traction and displacement, so long as these values are macroscopically uniform*". Technically speaking, this requires ergodic, stationary random fields of microscale properties, and what results is a macroscopic homogeneous continuum - i.e., the one whose effective moduli are not functions of position.

Studies of convergence to the RVE in the sense of Hill show that the effective (macroscopic) moduli are bounded from above (and below) by moduli obtained under uniform displacement (respectively, traction) controlled boundary conditions, that are applied on some finite sized windows. It has been shown from variational principles and homogenization theory [2, 3, 4] that the larger is the window, the closer are these bounds, and this trend has quantitatively been illustrated in 2-D anti- and in-plane elasticity, as well as 3-D elasticity. Thus, a question of great interest is this: how large is the difference between both bounds for finite windows at various degrees of mismatch between the moduli of constituent phases?

This is the basic motivation of the present study, and as shown in this paper for anti-plane elasticity, the difference between both bounds remains very significant indeed. When dealing with finite windows we call their properties *apparent moduli,* following [2], and treat them as the bases of inhomogeneous continuum models approximating the given microstructures on the chosen (finite) mesoscales [4, 5]. In other words, the mesoscale windows represent statistical volume elements (SVE), and provide a heretofore missing link to stochastic finite element methods; note that the classical, deterministic finite element method presupposes the existence of the RVE below (or

at) the scale of a single finite element [6].

Another definition of the RVE, different from that of Hill, has recently been introduced by Drugan and Willis [7]. According to them, the RVE is defined as "*the smallest material volume element of the composite for which the usual spatially constant 'overall modulus' macroscopic constitutive representation is a sufficiently accurate model to represent mean constitutive response.*" Their study involved a nonlocal correction to the effective property tensor in terms of the derivative of the average strain tensor field with respect to the slow coordinate. They found the minimum RVE size, in 3-D elasticity, to be on the order of just several inclusion diameters.

In this paper we study apparent moduli of unidirectional composites with cylindrical fibers, aligned in the axial direction, and arranged randomly, but with no overlap, in the transverse plane. We report new results on the effects of scale and boundary conditions on the elastic moduli by employing mesoscale continuum-type models. More specifically, we consider "windows of observation", which are on scales larger than a single fiber, yet smaller than the RVE in the sense of Hill [1]. To such mesoscale windows we apply different types of boundary conditions: displacement- and traction-controlled, used in Hill's definition, periodic boundary conditions, and mixed boundary conditions, involving combinations of the above three boundary conditions. We conduct our analysis numerically, using a spring network model [9], for a range of fiber-matrix moduli mismatch and several volume fractions. Note that our anti-plane problem is mathematically equivalent to other ones - e.g., thermal or electrical conductivity, or membrane problem - since they are all governed locally by a Laplace's equation.

The outline of this paper is as follows. First, in section 2 we present the model of the random composite, then in section 3 we discuss the boundary conditions. In section 4 we briefly describe the numerical method used. Finally, in section 5 we include our results on apparent elastic moduli and discussion, and in section 6 the conclusions are given.

2. Model of a Random Composite

We study the anti-plane elastic response of a unidirectional fiber composite material. The fibers are of circular cylinder shape, are aligned in the axial direction, and are randomly arranged in the transverse plane, with no overlap. A detail of a typical transverse cross-section of such a composite is shown in Fig. 1a. This is just one deterministic realization $B(\omega)$ of the random matrix-inclusion composite studied. The latter is taken as a set $\boldsymbol{B} = \{B(\omega)\,;\ \omega \in \Omega\}$, where ω is an element of the sample space Ω. Any $B(\omega)$ of the composite $\boldsymbol{B}$ (set of all $B(\omega)$'s) is, in the first place, described by a characteristic function

$$\chi_r(x, \omega) = \begin{cases} 1 & \text{if} \quad x \in B_r \\ 0 & \text{otherwise} \end{cases} \tag{2.1}$$

where B_r is body domain of phase $r\ (= i, m)$; $i\ (m)$ stands for the inclusion (matrix) phase. In our study we generate each ω realization by using a planar Poisson point process subject to a condition of inhibition. In this way we obtain a set of random points, which define centers of fibers. We accept each new point provided that it does not fall closer than a certain minimum distance with respect to any of the previous ones. This allows us to generate arrangements of random and non-overlapping fibers. In order to avoid the problem of arbitrarily narrow necks between inclusions, that would require a special numerical technique, we take the distance between the centers of inclusions to be 1.2 times greater than the inclusions' diameter d.

In our analysis we assume that the constitutive response of each of the phases $r\ (= i, m)$ in each $B(\omega)$ is elliptic

$$0 < \boldsymbol{e} \cdot \boldsymbol{C}^{(r)} \cdot \boldsymbol{e} < \infty \qquad \forall \boldsymbol{e} \neq \boldsymbol{0} \tag{2.2}$$

and linear elastic, isotropic

$$\sigma_i = C_{ij}\varepsilon_j \qquad i, j = 1, 2 \qquad C_{ij} = C^{(r)}\delta_{ij} \qquad r = i, m \tag{2.3}$$

where, for simplicity of notation, we denote

$$\sigma_i \equiv \sigma_{3i} \qquad \varepsilon_i \equiv \varepsilon_{3i} \qquad i, j = 1, 2 \tag{2.4}$$

Parallel to the subscript notation we shall also use the symbolic notation, so that, for example: $C_{ij} \equiv \boldsymbol{C}$.

The governing equation of our piecewise-constant material is

$$C\left(\frac{\partial^2 u}{\partial x_1^2} + \frac{\partial^2 u}{\partial x_2^2}\right) = 0 \qquad C = C^{(i)}, C^{(m)} \qquad u \equiv u_3 \tag{2.5}$$

Thus, $C = \{C(\boldsymbol{x}, \omega); \boldsymbol{x} \in B, \omega \in \Omega\}$ is a (scalar-valued) random field, such that

$$C(\boldsymbol{x}, \omega) = \sum_{r = i, m} C^{(r)} \chi_r(\boldsymbol{x}, \omega) \qquad \boldsymbol{x} \in B, \omega \in \Omega \tag{2.6}$$

where $B = B_m \cup B_i$ denotes the physical domain of every $B(\omega)$.

From the probability theory standpoint, this random field is specified via n-point probability distributions

$$P_n^C\{\boldsymbol{x}_1, \ldots, \boldsymbol{x}_n; I_1, \ldots, I_n\} \tag{2.7}$$

which gives the probability of simultaneously finding $C(\boldsymbol{x}_1, \omega)$ in I_1, $C(\boldsymbol{x}_2, \omega)$ in I_2, ... , and $C(\boldsymbol{x}_n, \omega)$ in I_n. Here $\boldsymbol{x}_1$, $\boldsymbol{x}_2$, ... , and $\boldsymbol{x}_n$ are arbitrary points in the transverse plane of the composite and I_1, I_2, ... , and I_n are arbitrary open intervals in the range of C.

It is well-known from the theory of random point fields that χ_r is homogeneous and has a mixing property, which is known to be a sufficient condition for it to be ergodic [10]. As a result, the random field $C(\boldsymbol{x}, \omega)$ is ergodic too.

Next, following Sab [3], let $F(B, \boldsymbol{A})$ represent a real functional of the open bounded domain B of volume V and random field $\boldsymbol{A}$ with the following five properties:

1. F is a property of the medium invariant with respect to any translation in the material domain.
2. For any partition of the domain B into n disjoint subdomains, F satisfies a subadditivity property

$$F(B, A) \leq \sum_{i=1}^{n} \frac{V_i}{V} F(V_i, A) \qquad B = \bigcup_{i=1}^{n} B_i \tag{2.8}$$

3. F is a measurable mapping with respect to the Ω sample space of outcomes ω.

4. A is a statistically homogeneous, ergodic random field.

5. F is uniformly bounded in B and ω in the sense that, there exists a real $b > 0$, such that

$$\forall B, \omega \qquad |F(B, A)| \leq b \tag{2.9}$$

Let us now take B to be a square-shaped domain, with side of length L, and which contains some microstructure of characteristic microscale d, e.g. Fig. 1(a). With the conditions 1-5 satisfied, we can adopt the result that there exists a non-random (i.e., deterministic) constant F^{Hom} such that, for all ω with probability one, we will have

$$\forall B, \omega \qquad \lim_{L/d \to \infty} F(B, A) = F^{Hom} \tag{2.10}$$

with the bound

$$\inf_{L/d} \langle F(B, A) \rangle = F^{Hom} \tag{2.11}$$

This limit is understood in the sense of the homogenization theory: $\boldsymbol{x} \to F^{\varepsilon}(\boldsymbol{x}) = F(\boldsymbol{x}/\varepsilon) \equiv F(\boldsymbol{y})$, where $\boldsymbol{x}$ and $\boldsymbol{y}$ are the so-called slow (macroscopic) and fast (microscopic) variables, respectively, and ε is a small parameter, reciprocal of our $\delta = L/d$.

If F represents the volume average elastic energy density or complementary energy density, then, $\boldsymbol{A}$ stands for the stiffness tensor of the domain B, and, from (2.11), one has

$$\sup_{L/d} \langle \boldsymbol{S} \rangle^{-1} = (\boldsymbol{S}^{Hom})^{-1} = \boldsymbol{C}^{Hom} = \inf_{L/d} \langle \boldsymbol{C} \rangle \tag{2.12}$$

where $(\boldsymbol{S}^{Hom})^{-1} = \boldsymbol{C}^{Hom}$ is the macroscopic (effective) stiffness tensor $\boldsymbol{C}^{eff}$ in the sense of Hill. However, (2.12) does not assert that $\langle \boldsymbol{S} \rangle^{-1}$ and $\langle \boldsymbol{C} \rangle$ are monotone functions of L/d; in fact, a scale-dependent hierarchy structure of the apparent properties is given in the next section.

3. Boundary Conditions

We study the scale dependent responses of our random composites numerically. We conduct our calculations in square regions of side L, which we call *windows*, e.g., [4, 6, 11]. The nondimensional parameter $\delta = L/d$ introduced in (2.10), where d is a diameter of a fiber, defines the *mesoscale* level. We investigate the effects of window size (in terms of δ) on the moduli predictions. Thus, if our random composite medium is parametrized by δ, we have $\boldsymbol{B}_\delta = \{B_\delta(\omega);\ \omega \in \Omega\}$. We shall study five scales $\delta = 3, 6, 12, 24, 48$ by computational mechanics and determine the corresponding apparent moduli and their statistics.

Effective elastic response of composites calculated over a finite domain will depend on the type of boundary conditions. The two basic ones used in predictions of effective elastic moduli are homogeneous boundary conditions with either controlled displacements or tractions for the anti-plane response tests under consideration here. They are given as follows:

Displacement (alternatively called kinematic, essential, or Dirichlet) uniform boundary condition (*dd*)

$$u(\boldsymbol{x}) = \varepsilon^0 \cdot \boldsymbol{x} \qquad \forall \boldsymbol{x} \in \partial B_\delta \tag{3.1}$$

and

Traction (alternatively called static, natural, or Neumann) uniform boundary condition (*tt*)

$$t(\boldsymbol{x}) = \sigma^0 \cdot \boldsymbol{n} \qquad \forall \boldsymbol{x} \in \partial B_\delta \tag{3.2}$$

Here ∂B_δ is a boundary of B_δ. With $u = u_3$ being the anti-plane displacement, $\varepsilon^0 = (\varepsilon_1^0, \varepsilon_2^0)$ is a given applied uniform strain, while t is the surface traction controlled by a given constant stress $\sigma^0 = (\sigma_1^0, \sigma_2^0)$; $\boldsymbol{n}$ is the unit outer normal to ∂B_δ.

The boundary condition (3.1) on ∂B_δ results in an apparent random stiffness tensor $\boldsymbol{C}_\delta(\omega)$, with the constitutive law

$$\bar{\sigma}(\omega) = \boldsymbol{C}_{\delta}(\omega) \cdot \varepsilon^{0} \tag{3.3}$$

The ω-dependence in (3.3) points to a random nature of the resulting average stress field (overbar indicates a volume average) and of the apparent stiffness tensor, with the fluctuations disappearing in the limit $\delta \to \infty$. Similarly, the boundary condition (3.2) on ∂B_{δ} results in an apparent random compliance tensor $S_{\delta}(\omega)$, with the constitutive law being stated as

$$\bar{\varepsilon}(\omega) = \boldsymbol{S}_{\delta}(\omega) \cdot \sigma^{0} \tag{3.4}$$

The third type of boundary conditions is a mixed condition, which involves a combination of (3.1) and (3.2). This condition may best represent experimental setups. It can be written as follows:

<u>*Displacement-traction*</u> boundary condition (*dt*)

$$(u(\boldsymbol{x}) - \varepsilon^{0} \cdot \boldsymbol{x}) \cdot (t(\boldsymbol{x}) - \sigma^{0} \cdot \boldsymbol{n}) = 0 \qquad \forall \boldsymbol{x} \in \partial B_{\delta} \tag{3.5}$$

In this paper, boundary conditions (3.5) are employed by specifying displacement boundary conditions on two parallel sides, and traction-free boundary conditions on the remaining two parallel sides.

Another aspect involves an assumption of finite scale periodicity in the microstructure. If we have such a microstructure - in a square-shaped window of length scale L (Fig. 1(b)) - we can specify periodic boundary conditions as follows:

<u>*Periodic*</u> boundary conditions (*pp*)

$$u(\boldsymbol{x} + \boldsymbol{L}) = u(\boldsymbol{x}) + \varepsilon^{0} \cdot \boldsymbol{L} \qquad t(\boldsymbol{x} + \boldsymbol{L}) = -t(\boldsymbol{x}) \qquad \forall \boldsymbol{x} \in \partial B_{\delta} \tag{3.6}$$

where $\boldsymbol{L} = L\boldsymbol{n}$.

Two other possibilities of mixed boundary conditions, considered in this paper, include combinations of boundary conditions (3.1), (3.2) and (3.6), namely

<u>*Displacement-periodic*</u> boundary conditions (*dp*), which is a combination of (3.1) and (3.6)

$$u(x) = \varepsilon^0 \cdot x \qquad \forall x \in \partial B_\delta^d$$
$$u(x+L) = u(x) + \varepsilon^0 \cdot L \qquad t(x+L) = -t(x) \qquad \forall x \in \partial B_\delta^p \tag{3.7}$$

<u>*Traction-periodic*</u> boundary conditions (*tp*), which involve (3.2) and (3.6)

$$t(x) = \sigma^0 \cdot n \qquad \forall x \in \partial B_\delta^t$$
$$u(x+L) = u(x) + \varepsilon^0 \cdot L \qquad t(x+L) = -t(x) \qquad \forall x \in \partial B_\delta^p \tag{3.8}$$

In equations (3.7) and (3.8) the superscripts *d*, *t* and *p* refer to displacement, traction, and periodic boundary conditions, respectively.

We apply these last two types of boundary conditions by subjecting two parallel sides of a square window to periodic conditions and the remaining two parallel edges to displacement- or traction-controlled boundary conditions, respectively.

Furthermore, we use windows with random, non-periodic geometry of the type shown in Fig. 1(a) when boundary conditions (3.1)-(3.3) are specified, and windows with a random, periodic geometry of periodicity *L*, shown in Fig. 1(b), when boundary conditions (3.6)-(3.8) are specified.

Given the random arrangement of fibers, a specimen's response on the mesoscale (δ finite) is, in general (i.e., with probability one), anisotropic. To quantify the degree of anisotropy, for either apparent response tensor - i.e., $\boldsymbol{C}_\delta$ or $\boldsymbol{S}_\delta$ - we employ the Mohr's circle radius *R*

$$R \equiv C_{12,\,max} = \sqrt{(C_{11} - C_{22})^2/4 + C_{12}^2} \tag{3.9}$$

We also use half of the trace $tr(\boldsymbol{C}_\delta)/2 \equiv C_{ii}/2$ to describe this tensor's fundamental magnitude.

The adoption of boundary conditions (3.1)-(3.2) leads - through the use of minimum potential and complementary energy principles along with the statistical homogeneity and ergodicity - to a *hierarchy of scale-dependent bounds* on the macroscopic stiffness tensor $\boldsymbol{C}^{eff}$, that is [2, 4]

$$\boldsymbol{C}^R \equiv (\boldsymbol{S}^R)^{-1} \equiv \langle \boldsymbol{S}_1^t \rangle^{-1} \le \langle \boldsymbol{S}_{\delta'}^t \rangle^{-1} \le \langle \boldsymbol{S}_\delta^t \rangle^{-1} \le \boldsymbol{C}^{eff} \le \langle \boldsymbol{C}_\delta^d \rangle \le \langle \boldsymbol{C}_{\delta'}^d \rangle \le \langle \boldsymbol{C}_1^d \rangle \equiv \boldsymbol{C}^V \qquad \forall \delta' = \delta/2 \tag{3.10}$$

In the above, C_δ^d and S_δ^t stand for apparent stiffness and compliance tensors on the scale δ, which were obtained under displacement (3.1) and traction (3.2) boundary conditions, respectively. The superscripts V and R refer to the Voigt and Reuss bounds, respectively. (3.10) had originally been proved for partitions, but an extension to more arbitrary systems has recently been given by [12].

4. Spring Network Discretization

Results reported in this paper are obtained by employing a spring network discretizing the composite in its transverse plane [9]. This type of method was first introduced in the condensed matter physics to simulate interatomic forces by springs. The primary advantage is that various types of heterogeneous media can easily be modeled by assigning the spring constants all over the lattice according to the local phase properties. For our composite material we employ a coarse square mesh lattice representation of continuum phases with 10 lattice spacings per disk diameter. This allows us to obtain results for large window sizes (up to $\delta = 48$) and the corresponding statistics using available computational resources (modern workstation).

The anti-plane stiffness tensor C_{ij} of a unit cell of this spring network, modeling an isotropic continuum, is related to the bond spring constant k as follows $C_{11} = C_{22} = k/2$. While placing the inclusions, we round off the coordinates of Poisson points so the disk centers are put on the nodes of the spring network. Next, we assign the spring constants of matrix and inclusion bonds (k^m and k^i) for each phase, while any bond crossing the circular matrix-inclusion boundaries has its spring constant k^b determined according to a series spring system weighted by the partial lengths (l^m and l^i) of the bond that belong to the respective domains, that is

$$k^b = \left(\frac{l^m}{lk^m} + \frac{l^i}{lk^i} \right)^{-1} \qquad l = |l^b| = l^m + l^i \tag{4.1}$$

We use a conjugate gradient method [13] with respect to the total energy (sum of energies stored in all the spring bonds) under either one of the boundary conditions (3.1-3.2), (3.5-3.8). The total elastic strain energy $U(V, \omega)$ stored in the network provides a basis for determination of the properties of an equivalent, homogenized medium. While we do not pursue the subject of fracture and damage of disordered composites, this spring network method provides a powerful tool for such studies as well [14].

5. Results and Discussion

In all our numerical simulations reported in this paper we applied anti-plane strain and/or stress fields. More specifically, we applied $\varepsilon^0 = (\varepsilon_1^0, 0)$ to calculate C_{11}, next we applied $\varepsilon^0 = (0, \varepsilon_2^0)$ to calculate C_{22}, and finally we applied $\varepsilon^0 = (\varepsilon_1^0, \varepsilon_2^0)$ to infer C_{12}. This was the procedure in cases of displacement (*dd*), displacement/traction (*dt*), periodic (*pp*), and displacement/periodic (*dp*) boundary conditions. On the other hand, in cases of traction (*tt*) and traction/periodic (*tp*) boundary conditions, to evaluate S_{11} we applied $\sigma^0 = (\sigma_1^0, 0)$, to evaluate S_{22} we applied $\sigma^0 = (0, \sigma_2^0)$, and finally we inferred S_{12} from the $\sigma^0 = (\sigma_1^0, \sigma_2^0)$ loading.

In order to investigate the effect of mesoscale (or, window size of observation) on overall elastic moduli we used five different window sizes: $\delta = L/d = 3, 6, 12, 24, 48$. To illustrate the effect of inclusion concentration on the overall moduli we considered two volume (i.e., area) fractions of inclusions $f = 10\%$ and 35% in Fig. 2 and in Fig. 4 we additionally included the results for $f = 45\%$. In all other figures we take volume fraction as $f = 35\%$. Since in this study we focus on composites with random arrangement of fibers, for each window size δ (scale) we run a number of realizations, see Table 1. The number of samples chosen in this study for each window size is sufficient for obtaining second order statistics [15].

Table 1: Window sizes and corresponding numbers of samples

Window size δ	3	6	12	24	48
Number of samples	300	200	100	50	20

In Fig. 2 we present results for the average of half of trace of the apparent anti-plane stiffness tensor, $tr(C_\delta)/2$, obtained using displacement (*dd*) and traction (*tt*) boundary conditions as a function of a scale of observation δ, ranging from 3 to 48 for two volume fractions $f = 10\%$ and 35% for four different stiffness ratios: (a) $C^{(i)}/C^{(m)} = 0.001$, (b) $C^{(i)}/C^{(m)} = 0.1$, (c) $C^{(i)}/C^{(m)} = 10$, and (d) $C^{(i)}/C^{(m)} = 1000$. This covers a wide range of materials from those with very soft inclusions to those with a very stiff reinforcement. Note that the values for traction-controlled boundary conditions were obtained by taking $(tr(S_\delta))^{-1}$.

The first observation from Fig. 2 is that the bounds become closer as the window size, i.e. δ increases. The displacement (*dd*) boundary conditions give an upper bound, while the traction boundary conditions give a lower bound, as expected. The actual character of the bounds strongly depends on which phase is softer and which is stiffer. When inclusions are soft the lower bounds tend to upper bound, while the opposite trend is observed for the case of inclusions stiffer than the matrix. This trend is consistent with what is suggested by the Hashin-Shtrikman bounds [16].

Another important issue concerns the rate of convergence of our bounds obtained from displacement and traction boundary conditions, respectively. We quantify this in terms of differences between the bounds as functions of the contrast by introducing two measures (see Table 2): $\left|C^d_{\delta=48} - C^t_{\delta=48}\right| / \left|C^V - C^R\right|$ and $\left|C^d_{\delta=48} - C^t_{\delta=48}\right| / \left|C^{(i)} - C^{(m)}\right|$ and summarize all the results in Table 2. These two measures are the ratios of discrepancy between the upper and lower bounds at $\delta = 48$ to the difference between either Voigt and Reuss bounds, or between the stiff-

nesses of individual phases, respectively. Note that both ratios decrease gradually as the stiffness mismatch $C^{(i)}/C^{(m)}$ increases, using the above measures, and the best convergence is achieved by materials with extremely stiff inclusions, while it is slowest for materials with very soft inclusions. In the singular case $C^{(i)}/C^{(m)} = 1$ the two measures are indeterminate.

Table 2: Differences between the bounds at $\delta = 48$

$\frac{C^{(i)}}{C^{(m)}}$	$\frac{\left\|C^{d}_{\delta=48} - C^{t}_{\delta=48}\right\|}{\left\|C^{V} - C^{R}\right\|}$	$\frac{\left\|C^{d}_{\delta=48} - C^{t}_{\delta=48}\right\|}{\left\|C^{(i)} - C^{(m)}\right\|}$
10^{-6}	0.742	0.482
0.001	0.482	0.312
0.01	0.123	0.0778
0.1	0.0203	0.0100
10	0.0100	0.00300
100	0.00710	0.00240
1000	0.00660	0.00230
10^{6}	0.00650	0.00228

In Fig. 3 we plot $\langle tr(\boldsymbol{C}_{\delta})\rangle/2$ calculated using six different boundary conditions (3.1-3.2) and (3.5-3.8) versus scale of observation δ when volume fraction is $f = 35\%$ for $C^{(i)}/C^{(m)} = 10$. Recall that for the first three types of boundary conditions, *dd*, *tt*, and *dt*, we used random unrestricted configurations of the type shown in Fig. 1(a), while for the remaining three boundary conditions, *dp*, *pp*, and *tp*, we used random microstructures with periodicity δ, according to Fig. 1(b).

In all our numerical examples, the results obtained using mixed boundary conditions (3.5-3.8), fall between the bounds obtained from displacement- and traction-controlled boundary value problems. Hazanov and Huet [17] obtained similar results in the context of in-plane elasticity. They showed analytically that apparent elastic stiffness, obtained using uniform displacement-traction

boundary conditions satisfying Hill's condition $\langle \sigma \cdot \varepsilon \rangle = \langle \sigma \rangle \cdot \langle \varepsilon \rangle$ [1], is bounded by displacement and traction boundary conditions predictions, at any scale δ, i.e.

$$\langle S_\delta^t \rangle^{-1} \leq \langle C_\delta^{dt} \rangle \leq \langle C_\delta^d \rangle \tag{5.1}$$

where C_δ^{dt} is the apparent stiffness tensor obtained using displacement-traction boundary conditions.

It is noted that the results obtained from displacement and traction boundary conditions are more sensitive to the window size than the results obtained from all other boundary conditions. In particular, results from periodic boundary condition remain almost unaffected by the change in window size. We find that under this boundary condition the window size of $\delta = 3$ is sufficient to estimate the effective moduli for mismatches ranging from 0.001 to 1000 (only the results of $C^{(i)}/C^{(m)} = 10$ are shown in Fig. 3). This observation is in agreement with the conclusions of Drugan and Willis [7] who showed that the window size of two or three times the diameter length can give very good estimates for effective stiffness. Their derivation, done in the context of three-dimensional elasticity, involved a random microstructure and, implicitly, periodic boundary conditions. Their results were verified numerically by Gusev [8] using FEM calculations of three dimensional periodic, random microstructures subjected to periodic boundary conditions.

In Fig. 4 we show a comparison of results for $<tr(C_\delta)/2>$ obtained using first and second order analytical bounds: Voigt upper bound (based on the assumption of a uniform strain in a composite) and Reuss lower bound (using the uniform stress assumption), and upper and lower bounds of Hashin and Shtrikman, and of results from our numerical simulations using displacement and traction boundary conditions for two different window sizes ($\delta = 6$ and $\delta = 48$) as a function of volume fraction f for stiffness mismatch $C^{(i)}/C^{(m)} = 0.01$. Note that the results of analytical bounds were calculated for the whole range of volume fractions from 0% to 100%. In our numer-

boundary conditions satisfying Hill's condition $\langle \sigma \cdot \varepsilon \rangle = \langle \sigma \rangle \cdot \langle \varepsilon \rangle$ [1], is bounded by displacement and traction boundary conditions predictions, at any scale δ, i.e.

$$\langle S_\delta^t \rangle^{-1} \leq \langle C_\delta^{dt} \rangle \leq \langle C_\delta^d \rangle \tag{5.1}$$

where C_δ^{dt} is the apparent stiffness tensor obtained using displacement-traction boundary conditions.

It is noted that the results obtained from displacement and traction boundary conditions are more sensitive to the window size than the results obtained from all other boundary conditions. In particular, results from periodic boundary condition remain almost unaffected by the change in window size. We find that under this boundary condition the window size of $\delta = 3$ is sufficient to estimate the effective moduli for mismatches ranging from 0.001 to 1000 (only the results of $C^{(i)}/C^{(m)} = 10$ are shown in Fig. 3). This observation is in agreement with the conclusions of Drugan and Willis [7] who showed that the window size of two or three times the diameter length can give very good estimates for effective stiffness. Their derivation, done in the context of three-dimensional elasticity, involved a random microstructure and, implicitly, periodic boundary conditions. Their results were verified numerically by Gusev [8] using FEM calculations of three dimensional periodic, random microstructures subjected to periodic boundary conditions.

In Fig. 4 we show a comparison of results for $<tr(C_\delta)/2>$ obtained using first and second order analytical bounds: Voigt upper bound (based on the assumption of a uniform strain in a composite) and Reuss lower bound (using the uniform stress assumption), and upper and lower bounds of Hashin and Shtrikman, and of results from our numerical simulations using displacement and traction boundary conditions for two different window sizes ($\delta = 6$ and $\delta = 48$) as a function of volume fraction f for stiffness mismatch $C^{(i)}/C^{(m)} = 0.01$. Note that the results of analytical bounds were calculated for the whole range of volume fractions from 0% to 100%. In our numer-

ical simulations we only considered three different volume fractions: f = 10%, 35%, and 45%. For the geometries considered in this paper, involving randomly arranged but non-overlapping circular fibers, we did not generate results for higher volume fractions due to large computer time and limits due to maximum packing. At volume fractions close to maximum packing it would take very long time to generate a family of samples. In the graphs illustrating numerical results for each case we connect the each three points obtained numerically by straight lines and end results at volume fraction of 1 at which we assume the effective properties to be those of the inclusions.

In Fig 4 we can see that the Voigt and Reuss bounds are very wide and so are the Hashin-Shtrikman bounds. The results of our numerical simulations fall close to the Hashin-Shtrikman upper bound. Note that except for the lower bound for $\delta = 6$, the bounds obtained numerically are close to the Hashin-Shtrikman upper bound, and the bounds obtained for $\delta = 48$ are much closer to each other and they fall between the bounds obtained from $\delta = 6$ calculations. When the inclusions are stiffer than the matrix, our results of numerical simulations fall close to the Hashin-Shtrikman lower bound. Again the results for $\delta = 48$ are between those of $\delta = 6$ [15].

In Fig. 5 we address the issue involving the geometry. In particular we focus on the difference between cases shown in Fig. 1(a) and 1(c). In Fig. 1(a) we consider a window placed on a random arrangement of fibers and have no restriction on whether the fibers cut across the boundaries or not. We refer to this case as sampling 1. In Fig. 1(c), on the other hand, we generate a microstructure in such a way that no inclusion falls on the boundary; we refer to this situation as sampling 2. In Fig. 5 we compare $<tr(\boldsymbol{C}_\delta)/2>$ obtained for these two types of microstructures using traction and displacement boundary conditions. In Fig. 5(a) we consider the case when inclusions are softer than the matrix $(C^{(i)}/C^{(m)} = 0.01)$, while in Fig. 5(b) the case when inclusions are stiffer $(C^{(i)}/C^{(m)} = 100)$. For each data point, i.e., each δ, boundary condition, and stiffness mismatch we again calculate results for a number of realizations (samples), as specified in Table 1. It is interesting to observe that the bounds obtained from geometries of Fig. 1(c) are much closer to each

other than those obtained using the type of geometry shown in Fig. 1(a). This is true for both mismatches. The numerical results obtained using geometry of Fig. 1(c) are less dependent on the window size and for these two mismatches the δ as low as 12 gives quite narrow bounds. We may point out here that both types of geometries are realistic. The example of case shown in Fig. 1(a) is a window taken using a typical composite cross-section. The case of Fig. 1(c) may be realized, for example, by casting a concrete specimen. In that case the aggregates (inclusions) will not cross the boundary, unless we will cut the specimen.

We are also interested in the coefficients of variation (CV) of $tr(\boldsymbol{C}_\delta)/2$ and $tr(\boldsymbol{S}_\delta)/2$ versus scale δ for a range of stiffness mismatches at volume fraction $f = 35\%$. Basically, as the window size δ increases, the CVs of $tr(\boldsymbol{C}_\delta)/2$ and $tr(\boldsymbol{S}_\delta)/2$ decrease. From our results, we found that, under displacement condition, for a fixed size window, the scatter of $tr(\boldsymbol{C}_\delta)/2$ is highest for materials with very stiff fibers, i.e., $C^{(i)}/C^{(m)} = 10^6, 10^3$, among all the cases. While under traction condition, for a fixed size window, the scatter of $tr(\boldsymbol{S}_\delta)/2$ is highest for materials with very soft inclusions, $C^{(i)}/C^{(m)} = 10^{-6}, 10^{-3}$, among all the cases. In Fig. 6, where mixed boundary conditions are applied, the CV is much less dependent on the stiffness mismatch and the range is narrower comparing with the results under displacement and traction conditions.

Finally, we study the characteristics of R. We found that when the scale of observation is small, the anisotropy effects are most pronounced; they diminish with the increase in window size, as expected. In Fig. 7, we show CV(R) under displacement condition. The CV(R) remains almost constant (around 0.6-0.7). In addition, it is insensitive to the mismatch in stiffness of phases' moduli. The CV(R) under traction condition, which is not shown here, looks almost the same as that under displacement condition. Upon a closed examination, we see that CV(R) makes a slight "dip" around $\delta = 10$ to 20, and then comes back up at large scales. This behavior is due to the fact that composite in the present study is generated by a hard-core process, which is not a Poisson point

process precisely, but its modification. The independence of CV(R) of the window scale has been observed in several other microstructures generated by Poisson point processes [6, 11, 12].

6. Conclusions

In this paper we evaluated apparent anti-plane elastic moduli (moduli calculated at scales smaller than the representative volume element) of unidirectional fiber reinforced composites and studied the effect of scale of observation and boundary conditions on these moduli. This investigation may be summarized as follows:

1. While we confirm that the scale dependent bounds stemming from the displacement and traction boundary conditions become closer as the window size increases, they remain very wide for window sizes even 50 times larger than the inclusion diameter. For materials with very soft inclusions these bounds have the slowest convergence. This sheds light on the RVE size according to the classical definition of Hill [1].
2. Results for apparent elastic moduli calculated using traction-displacement, periodic, periodic-displacement, and traction-displacement controlled boundary conditions fall between the bounds obtained by applying displacement and traction boundary conditions. These results are less sensitive to changing window size especially at larger scales.
3. When a microstructure is represented in such a way that inclusions don't cross boundaries the bounds obtained using essential and natural boundary conditions are much tighter than those obtained using cross-sections with fibers crossing boundaries.
4. The coefficient of variation of apparent elastic modulus decreases as window size increases.
5. The coefficient of variation of R, measure of the degree of anisotropy, is insensitive to changing scale and stiffness mismatch for displacement and traction boundary conditions.

Acknowledgments

This research was supported by the NSF under grants CMS-9713764 and CMS-9753075.

References

[1] Hill, R. (1963), Elastic properties of reinforced solids: some theoretical principles, *J. Mech. Phys. Solids* **11**, 357-372.

[2] Huet, C. (1990), Application of variational concepts to size effects in elastic heterogeneous bodies, *J. Mech. Phys. Solids* **38**, 813-841.

[3] Sab, K. (1992), On the homogenization and the simulation of random materials, *Eur. J. Mech. A/Solids* **11**(5), 583-607.

[4] Ostoja-Starzewski, M. (1993), Micromechanics as a basis of random elastic continuum approximations, *Probabilistic Eng. Mech.* **8**, 107-114.

[5] Ostoja-Starzewski, M. (1994), Micromechanics as a basis of continuum random fields, *Appl. Mech. Rev.* **47**(1, Part 2), S221-S230.

[6] Ostoja-Starzewski, M. (1999), Microstructural disorder, mesoscale finite elements, and macroscopic response, *Proc. Roy. Soc. Lond. A* **455**, 3189-3199.

[7] Drugan, W.J. and Willis, J.R. (1996), A micromechanics-based non-local constitutive equation and estimates of representative volume element size for elastic composites, *J. Mech. Phys. Solids* **44**, 497-524.

[8] Gusev, A.A. (1997), Representative volume element size for elastic composites: a numerical study, *J. Mech. Phys. Solids* **45**, 1449-1459.

[9] Ostoja-Starzewski, M., Sheng, P.Y., and Alzebdeh, K. (1996), Spring network models in elasticity and fracture of composites and polycrystals, *Comp. Mater. Sci.* **7** (1&2), 82-93.

[10] Stoyan, D. and Stoyan, H. (1994), *Fractals, Random Shapes and Point Fields*, John Wiley & Sons.

[11] Ostoja-Starzewski, M. (1998), Random field models of heterogeneous materials, *Intl. J. Solids Struct.* **35**(19), 2429-2455.

[12] Ostoja-Starzewski, M. (1999), Scale effects in materials with random distributions of needles and cracks, *Mech. Mater.* **31**, 883-893.

[13] Press, W.H., Teukolsky, S.A., Vetterling, W.T. and Flannery, B.P. (1992), *Numerical Recipes*, Cambridge University Press.

[14] Alzebdeh, K., Al-Ostaz, A., Jasiuk, I., and Ostoja-Starzewski, M. (1998), Fracture of random matrix-inclusion composites: scale effects and statistics, *Int. J. Solids Struct.* **35**, 2537-2566.

[15] Jiang, M. (2000), Scale and boundary conditions effects in fiber-reinforced composites, Georgia Institute of Technology, Ph.D. dissertation.

[16] Hashin Z. (1983), Analysis of composite materials - A survey, *J. Appl. Mech.*, 50, 481-505.

[17] Hazanov S. and Huet C. (1994), Order relationships for boundary conditions effect in the heterogeneous bodies smaller than the representative volume, *J. Mech. Phys. Solids* **42**, 1995-2011.

Figure legends

Fig. 1(a) Matrix-inclusion composite with randomly arranged, non-overlapping inclusions of diameter d and a square window of observation with a side of length L, the scale is defined by $\delta = L/d$; (b) a periodic window of scale $\delta = L/d$; (c) a window of a random composite with no inclusions crossing the boundary.

Fig. 2 Ensemble average of half of trace of the apparent anti-plane stiffness tensor $\langle tr(\boldsymbol{C}_\delta)/2 \rangle$ obtained using displacement-controlled (*dd*) and traction-controlled (*tt*) boundary conditions as a function of a scale of observation δ for two volume fractions $f = 10\%$ and 35% when (a) $C^{(i)}/C^{(m)} = 0.001$, (b) $C^{(i)}/C^{(m)} = 0.1$, (c) $C^{(i)}/C^{(m)} = 10$, and (d) $C^{(i)}/C^{(m)} = 1000$.

Fig. 3 Effect of boundary conditions: displacement-controlled (*dd*), traction-controlled (*tt*), periodic (*pp*), and mixed (displacement-periodic (*dp*), displacement-traction (*dt*), and traction-periodic (*tp*)) on the half of trace of the apparent anti-plane stiffness tensor $\langle tr(\boldsymbol{C}_\delta)/2 \rangle$ as a function of a scale of observation δ when volume fraction $f = 35\%$ and $C^{(i)}/C^{(m)} = 10$.

Fig. 4 Bounds on $\langle tr(\boldsymbol{C}_\delta)/2 \rangle$ as functions of volume fraction f for $C^{(i)}/C^{(m)} = 0.01$.

Fig. 5 $\langle tr(\boldsymbol{C}_\delta)/2 \rangle$ versus scale δ for two types of microstructure (sampling 1, shown in Fig. 1(a); sampling 2 - Fig. 1(c)) when volume fraction $f = 35\%$ for (a) $C^{(i)}/C^{(m)} = 0.01$ and (b) $C^{(i)}/C^{(m)} = 100$.

Fig. 6 $CV[tr(\boldsymbol{C}_\delta)/2]$ as a function of scale δ under *dt* boundary condition.

Fig. 7 Coefficient of variation of R as a function of window size δ under displacement boundary condition.

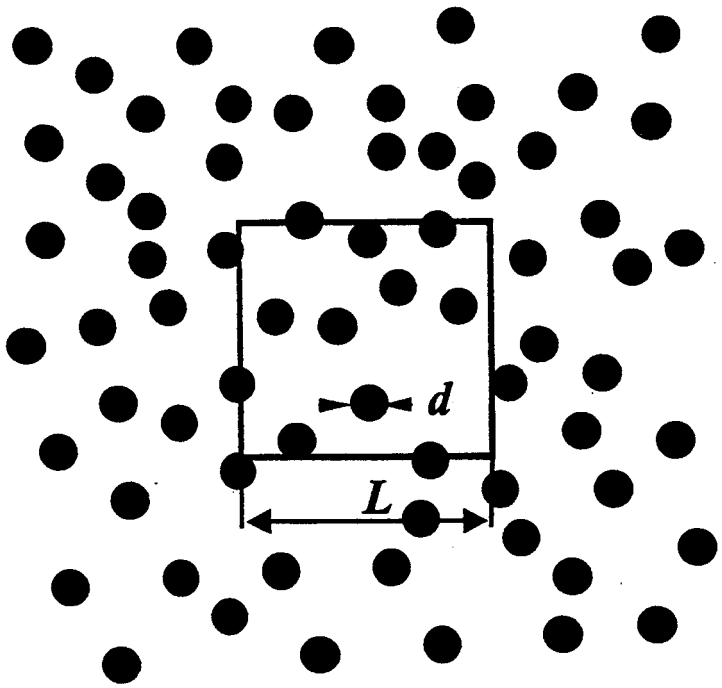

(a)

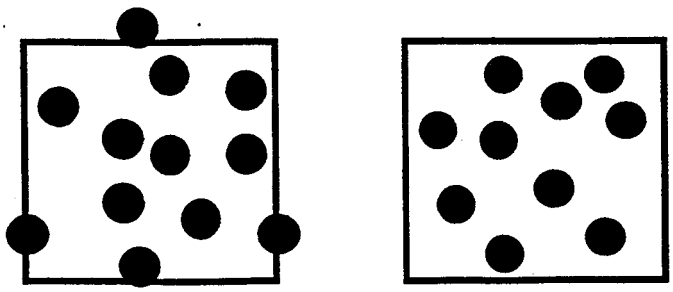

(b) (c)

Figure 1

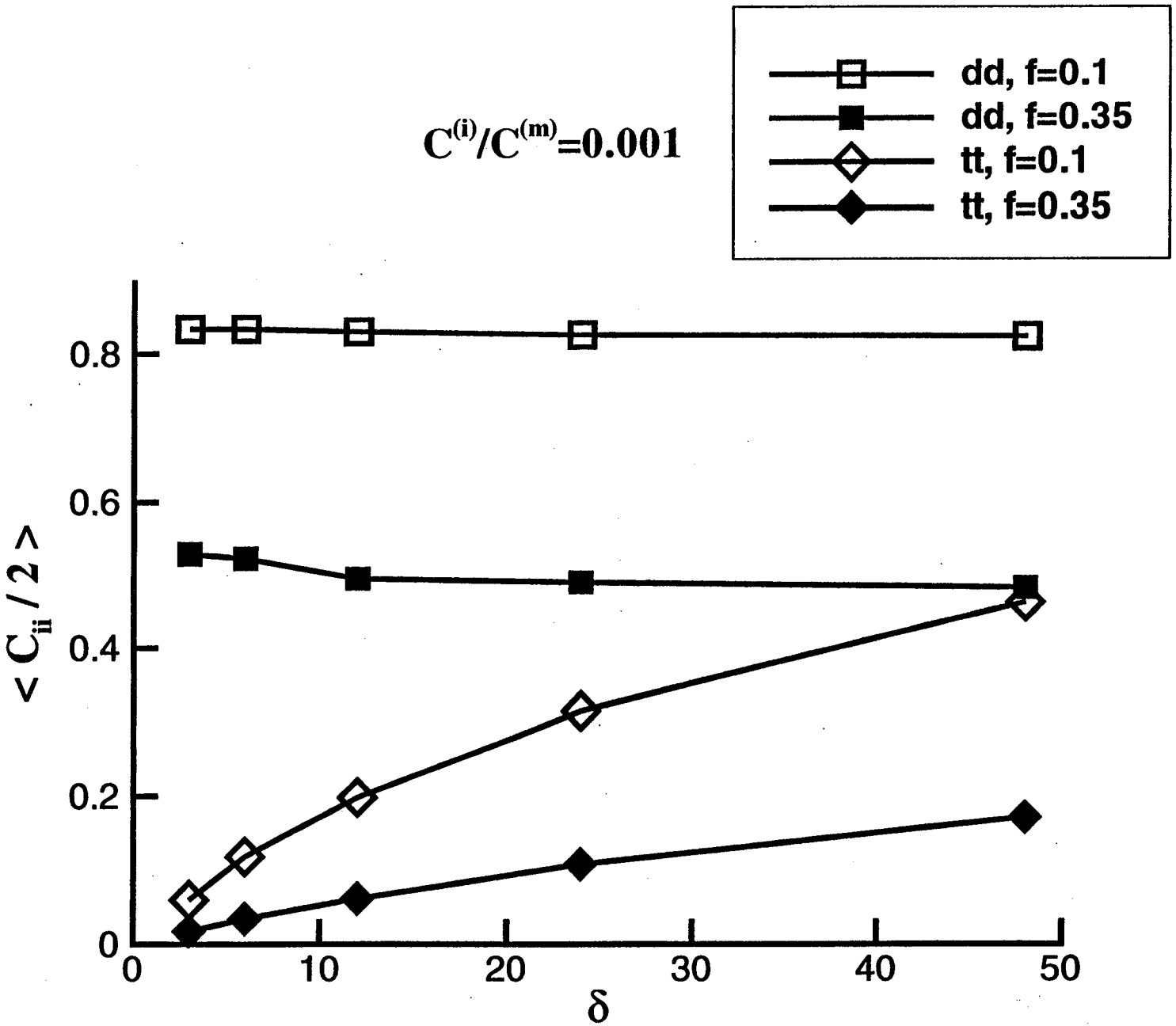
$C^{(i)}/C^{(m)}=0.001$
dd, f=0.1
dd, f=0.35
tt, f=0.1
tt, f=0.35
0.8
0.6
0.4
0.2
0
$< C_{ii} / 2 >$
0
10
20
30
40
50
δ

Figure 2(a)

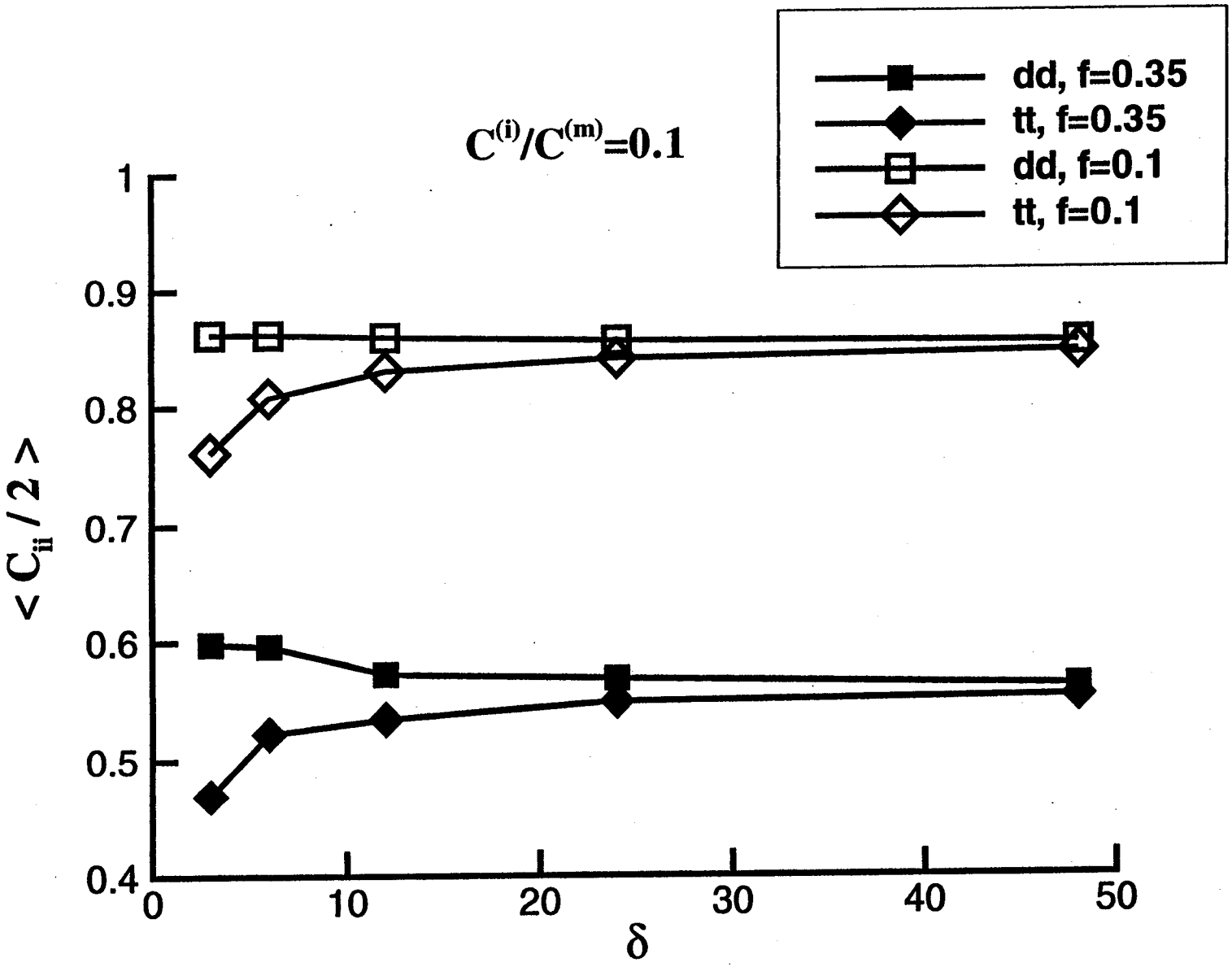
$C^{(i)}/C^{(m)}=0.1$
dd, f=0.35
tt, f=0.35
dd, f=0.1
tt, f=0.1
$< C_{ii} / 2 >$
1
0.9
0.8
0.7
0.6
0.5
0.4
0
10
20
30
40
50
δ

Figure 2(b)

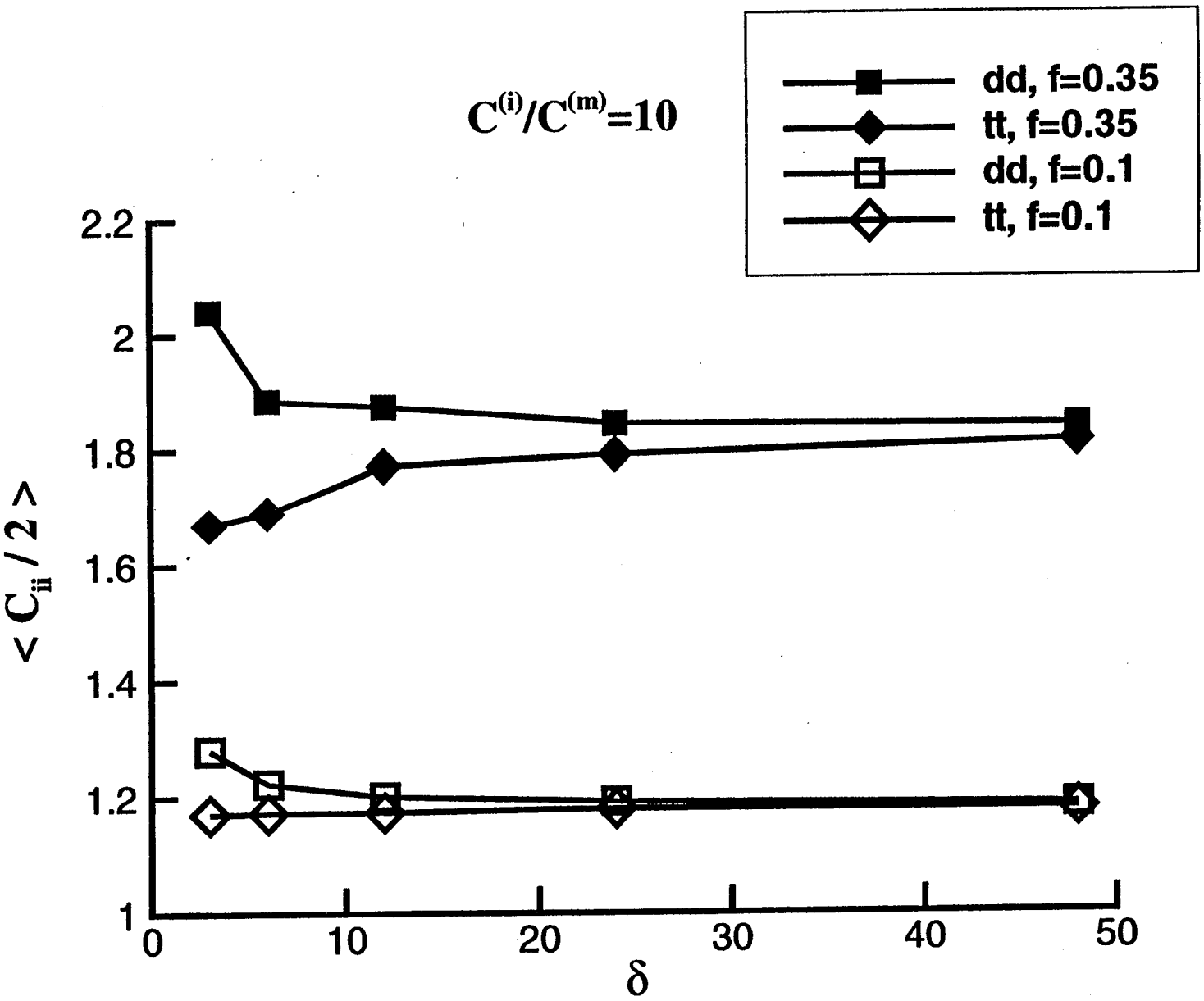
$C^{(i)}/C^{(m)}=10$
dd, f=0.35
tt, f=0.35
dd, f=0.1
tt, f=0.1
$< C_{ii} / 2 >$
2.2
2
1.8
1.6
1.4
1.2
1
0
10
20
30
40
50
δ

Figure 2(c)

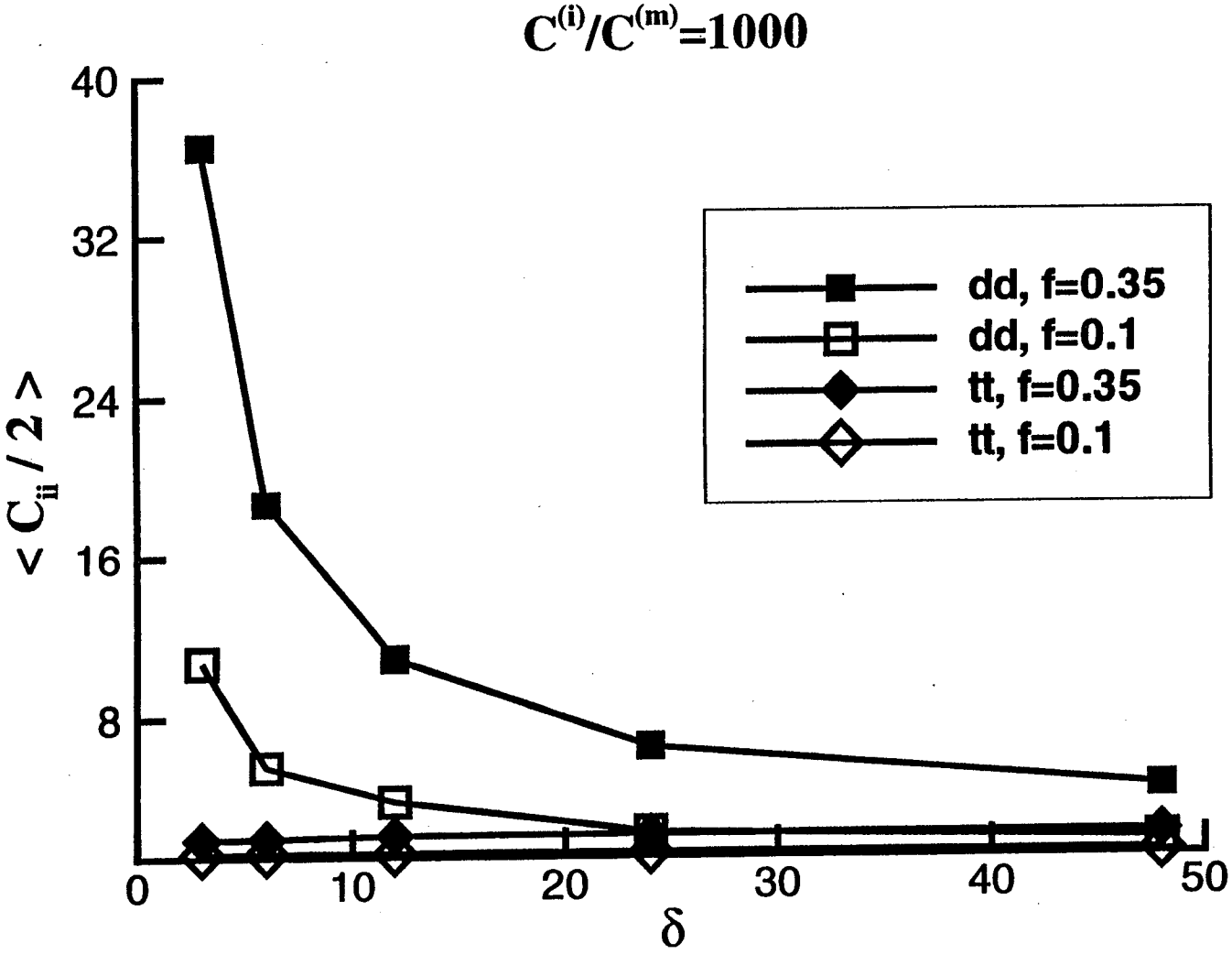
$C^{(i)}/C^{(m)}=1000$
40
32
24
16
8
0
10
20
30
40
50
$< C_{ii} / 2 >$
δ
dd, f=0.35
dd, f=0.1
tt, f=0.35
tt, f=0.1

Figure 2(d)

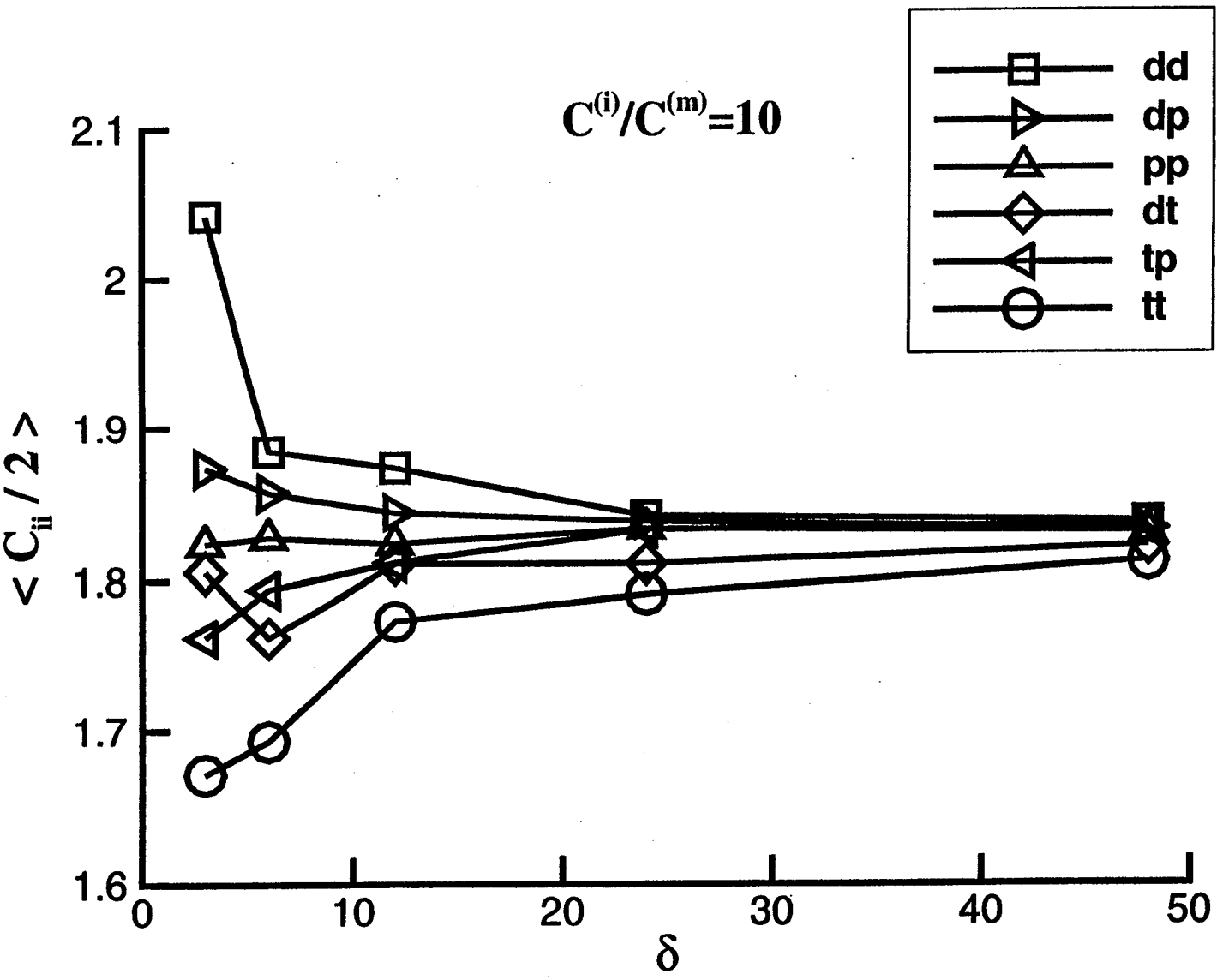

Figure 3

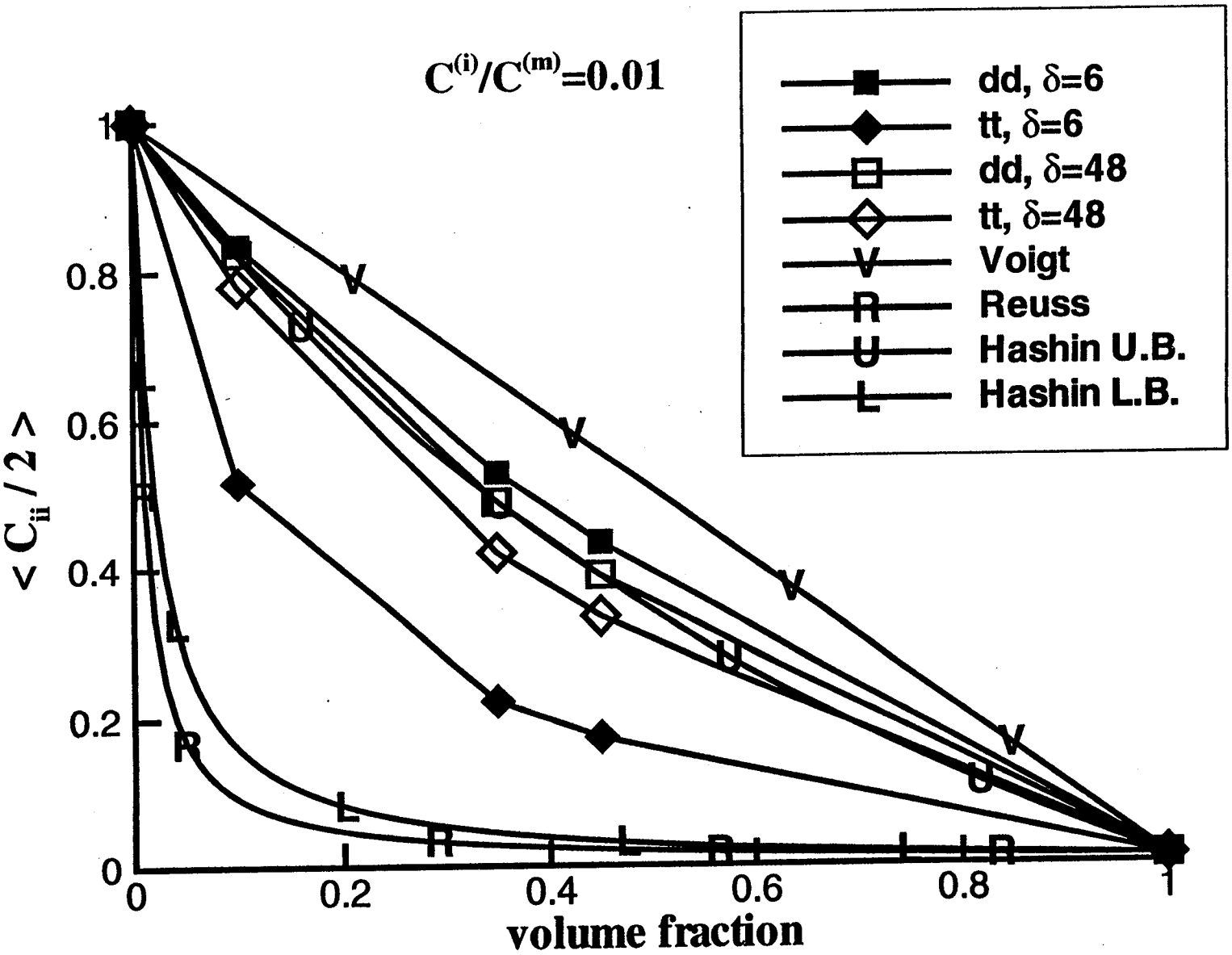
$C^{(i)}/C^{(m)}=0.01$
dd, δ=6
tt, δ=6
dd, δ=48
tt, δ=48
Voigt
Reuss
Hashin U.B.
Hashin L.B.
$< C_{ii} / 2 >$
volume fraction
0
0.2
0.4
0.6
0.8
1

Figure 4

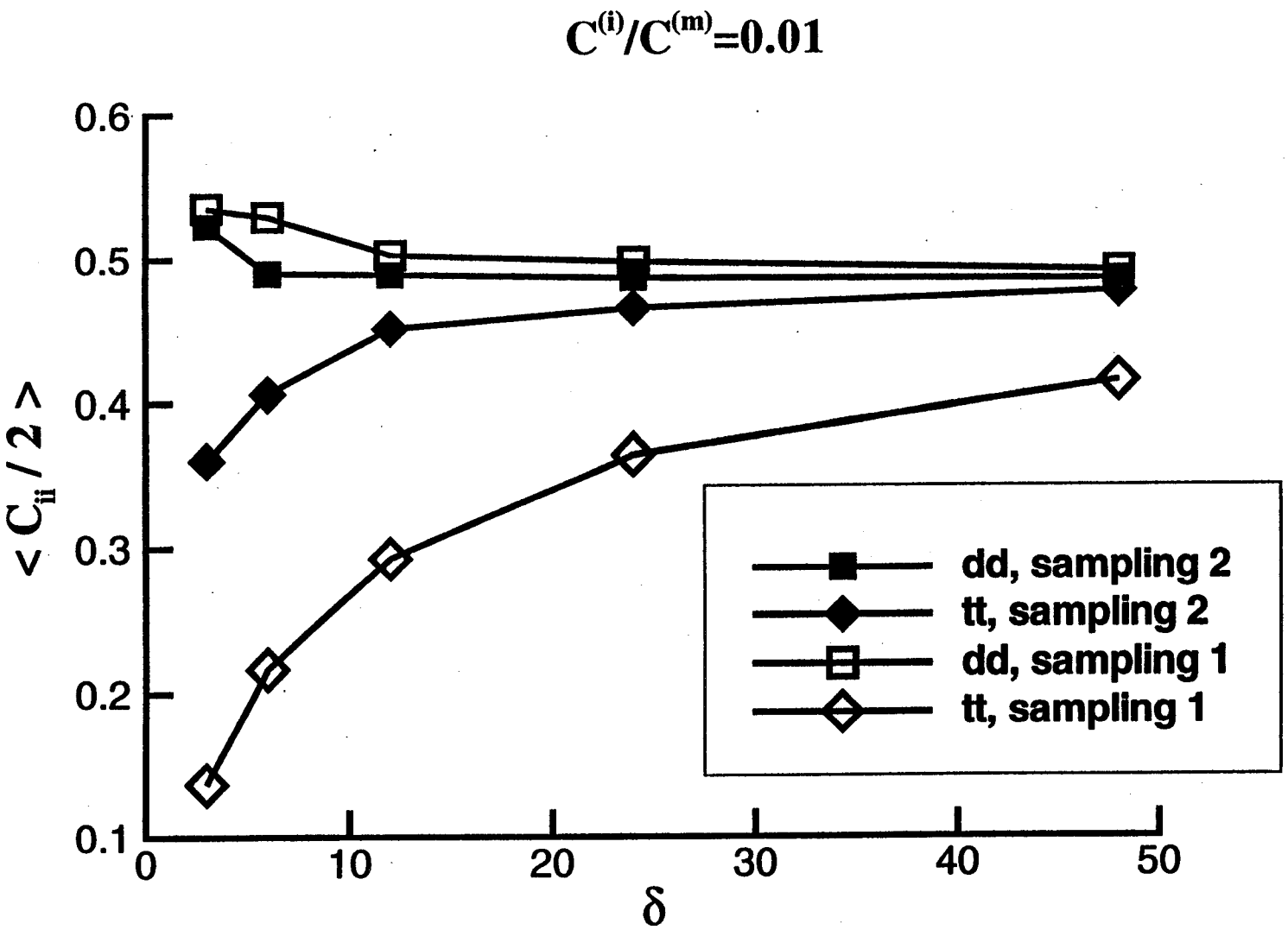
$C^{(i)}/C^{(m)}=0.01$
0.6
0.5
0.4
0.3
0.2
0.1
$< C_{ii} / 2 >$
0
10
20
30
40
50
δ
dd, sampling 2
tt, sampling 2
dd, sampling 1
tt, sampling 1

Figure 5(a)

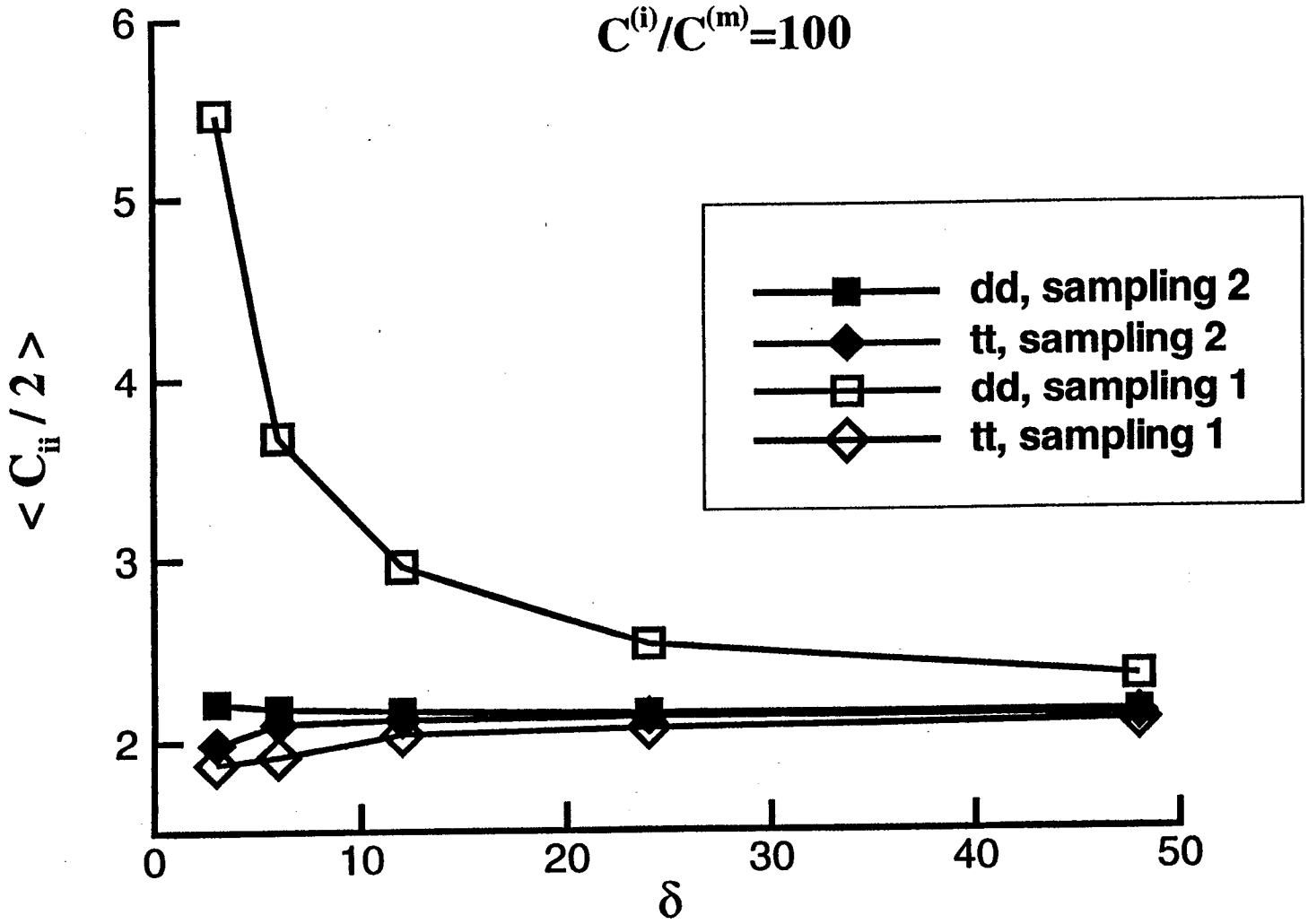
$C^{(i)}/C^{(m)}=100$
$< C_{ii} / 2 >$
6
5
4
3
2
0
10
20
30
40
50
δ
dd, sampling 2
tt, sampling 2
dd, sampling 1
tt, sampling 1

Figure 5(b)

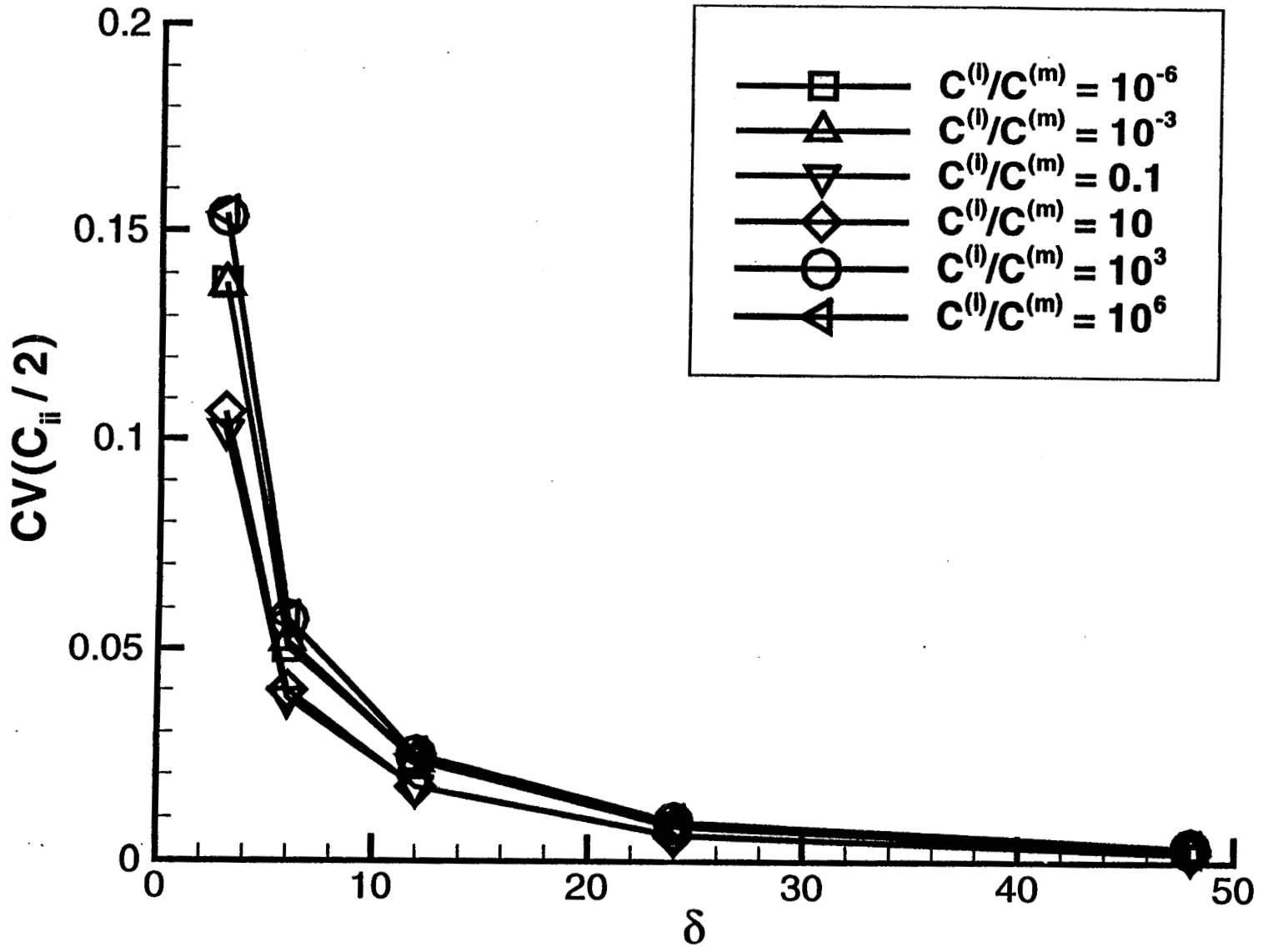
0.2
0.15
0.1
0.05
0
CV(C_ii / 2)
0
10
20
30
40
50
δ
C(l)/C(m) = 10-6
C(l)/C(m) = 10-3
C(l)/C(m) = 0.1
C(l)/C(m) = 10
C(l)/C(m) = 103
C(l)/C(m) = 106

Figure 6

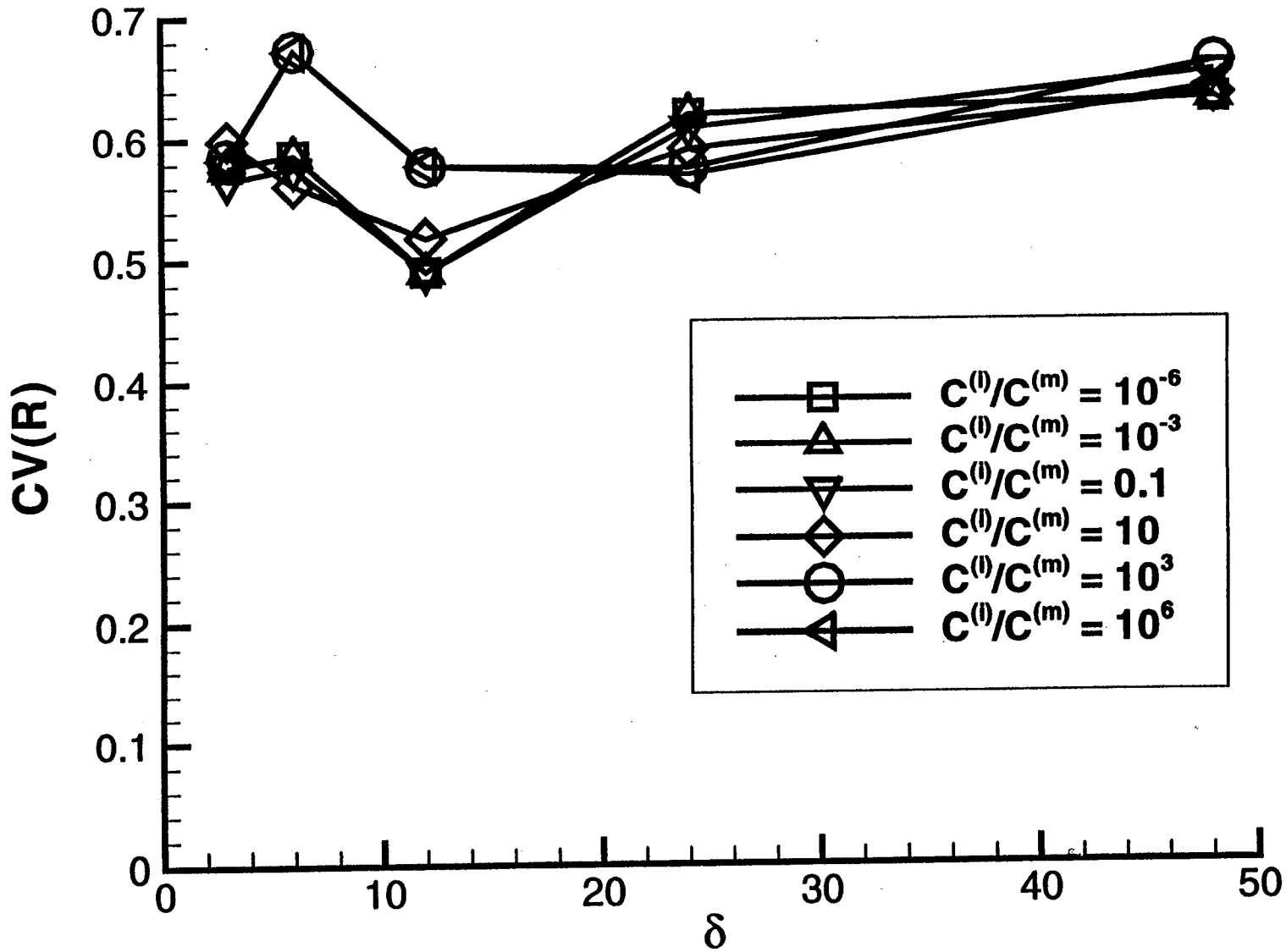
0.7
0.6
0.5
0.4
0.3
0.2
0.1
0
CV(R)
0
10
20
30
40
50
δ
C(i)/C(m) = 10-6
C(i)/C(m) = 10-3
C(i)/C(m) = 0.1
C(i)/C(m) = 10
C(i)/C(m) = 10³
C(i)/C(m) = 10⁶

Figure 7